ChemComm

COMMUNICATION

Supramolecular pathway selection of perylenediimides mediated by chemical fuels

Received 00th January 20xx,
Accepted 00th January 20xx

DOI: 10.1039/x0xx00000x

www.rsc.org/

Jorge Leira–Iglesias,[a] Alessandro Sorrenti,[a] Akihiro Sato,[a] Peter A. Dunne,[a] and Thomas M. Hermans*,[a]

We demonstrate supramolecular pathway selection of a perylenediimide derivative in aqueous solution using chemically fueled redox reactions to control assembly / disassembly cycles. The number and frequency of cycles affect the nucleation and growth process, providing control over the size and internal order of the resulting self-assembled structures.

Self-assembly of small molecules has been used to obtain well-ordered supramolecular polymers and assemblies with exciting applications in fields ranging from materials science to nanomedicine.[1,2] For assemblies governed by reversible non-covalent interactions (e.g., hydrogen bonding or π–π interactions) their size and structure are often dictated by the thermodynamic equilibrium (i.e., the global minimum in free energy). However, when strong non-covalent interactions are involved, the kinetics of self-assembly will determine whether the equilibrium state can be reached in the first place (i.e., the assemblies can reside in local minima), and whether this occurs on a reasonable time-scale.[3] In recent years kinetic studies on self-assembling systems have provided new mechanistic insights (e.g., nucleation effects, or the presence of multiple coupled assembly equilibria), and have extended the toolbox of non-covalent synthesis by making use of pathway complexity.[3–6] In other words, the sequence and rate of experimental actions (e.g., dilution, heating/cooling, stirring/shaking) is very important for the outcome of the self-assembly process. The latter is particularly relevant in aqueous environments where assembly is dominated by the hydrophobic effect, resulting in high kinetic barriers and slow exchange dynamics.[3,7] Recent examples of supramolecular pathway selection approaches include: optimized solvent processing,[3,8] stepwise non-covalent synthesis,[9,10] controlled diffusion,[11] application of hydrodynamic fields[12] and living non-covalent polymerization.[13] Most of these approaches use well-controlled heating/cooling steps to obtain kinetic control.[3–5,14]

However, in aqueous media such steps are often hampered by the hydrophobic effect, where heating leads to aggregation[15,16] or precipitation due to entropic effects.[7]

Here we demonstrate a new approach, where pathway selection is mediated by two redox agents that fuel assembly / disassembly cycles of a perylenediimide derivative in water. In this way we can circumvent strong kinetic trapping notorious for PDI-based systems.[3,14] Moreover, the number of redox cycles, as well as the rate of the cycles, determine the final structure of the assemblies, controlling the balance between colloidal stability and precipitation.

Perylenediimides (PDI's) are among the most versatile building blocks for supramolecular architectures, with applications in organic electronics, photovoltaics or as smart materials.[17,18] Facile synthesis, distinct spectroscopic / redox properties, outstanding stability (even in the reduced and oxidized forms), and great propensity to self-assemble both in solution and on surfaces make PDI's an attractive platform to study self-assembly and to obtain innovative materials.[18] The extended π-surface of PDI causes strong self-assembly in aqueous solution with assembly constants at least two orders of magnitude higher than in any other solvent.[19] Due to their electron-deficient character, PDI's can be easily reduced in a stepwise reversible process generating a stable doubly reduced dianion, via the unstable radical anion (cf. section 3, ESI†).[20] In addition, PDI's can be chemically reduced by sodium dithionite ($Na_2S_2O_4$) in aqueous media (Fig. 1a) forming stable dianions that can be oxidized back upon exposure to air.[21–23] Such redox reactions were previously used to obtain a reversible PDI-based hydrogel,[24] or crystalline PDI nanobelts.[25]

We synthesized symmetric **PDI-1** (Fig. 1a), containing solubilizing oligoethyleneglycol chains and H-bond forming amide-moieties by imidization of perylene-3,4,9,10-tetracarboxylic acid dianhydride with ethylenediamine, followed by peptide coupling with an oligoethyleneglycol derivative of gallic acid (section 1, ESI†). **PDI-1** dissolved promptly in aqueous 50 mM borate buffer (pH 8), up to a concentration of 100 µM, giving homogeneous solutions with a cherry red colour characteristic for PDI's.

[a] *Institut de Science et d'Ingénierie Supramoléculaires (ISIS) UMR 7006, Université de Strasbourg, CNRS & icFRC. 8 allée Gaspard Monge 67000 Strasbourg, France.*
[b] *E-mail: hermans@unistra.fr*

†Electronic Supplementary Information (ESI) available: synthesis & methods, electrochemical analysis, UV-Vis / fluorescence of **PDI-1** and **PDI-1**$^{2-}$, self-assembly studies of **PDI-1**$^{2-}$, AFM images, study of autocatalytic growth of **PDI-1** assemblies. See DOI: 10.1039/x0xx00000x

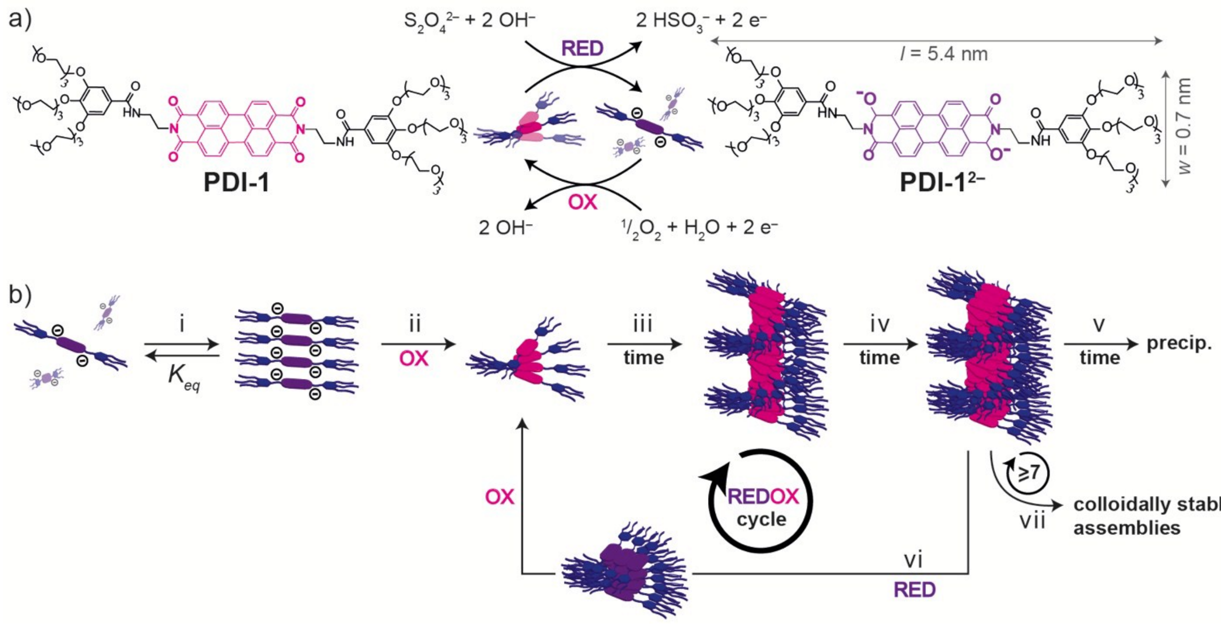

Fig. 1 (a) Typical redox cycle of **PDI-1.** The neutral **PDI-1** is reduced by $Na_2S_2O_4$ to **PDI-1**$^{2-}$, which can be oxidized back by O_2. (b) Schematic representation of pathway selection with the following steps: i) equilibrium between monomeric and assembled **PDI-1**$^{2-}$, ii) oxidation followed by internal structural rearrangement, iii–iv) nucleation and growth of side–to–side fused assemblies, v) precipitation (overnight), vi) reduction by $Na_2S_2O_4$ followed by O_2 oxidation, resulting in 1 redox cycle, vii) alternative pathway yielding colloidally stable aggregates by 7 or more redox cycles at a suitable frequency (see main text).

However, after overnight ageing precipitation was observed. In addition, heating the solution lead to rapid precipitation and can therefore not be used to obtain soluble assemblies. The UV-Vis spectra of freshly prepared **PDI-1** solutions showed a broad absorption (400–650 nm) due to the S0→S1 transition of the PDI core, with maxima at 505, 525, and 560 nm (Fig. S2a, ESI†). The broad band lacks the characteristic vibronic structure of monomeric PDIs, and strongly indicates **PDI-1** aggregation due to π–π stacking (H-aggregation).[18,19,26,27] In addition, no monomeric **PDI-1** could be detected by fluorescence spectroscopy (Fig. S2b), and a markedly red-shifted emission was observed, which is characteristic for cofacially stacked PDIs (cf. spectra of monomeric **PDI-1**, Fig. S3, ESI†).[18,28] Lastly, confocal micrographs (using a spectral detector) confirmed the presence of large red emissive aggregates, with a broad size distribution centred at ~5 μm (Fig. 2a,c). In other words, dissolution of as-synthesized **PDI-1** in buffer yields large colloidal π–π stacked assemblies that precipitate slowly overnight.

Upon addition of 2 eq. $Na_2S_2O_4$ solution (1 μL) to 100 μM **PDI-1** (2 mL) in borate buffer, an abrupt colour change from red to purple was observed, indicative of the formation of **PDI-1**$^{2-}$ (Movie M1, ESI†). This visual colour change coincided with a hyperchromic effect in the UV-Vis spectrum, where an intense band with partially resolved vibronic structure (maxima at 509 and 543 nm), together with a weaker band at 614 nm, appeared (Fig. S2a, ESI†), indicative of PDI dianions in water.[21,22] However, the ratio of the peak intensities I_{509nm}/I_{543nm} for **PDI-1**$^{2-}$ is higher (0.78) as compared to previous reports[21,22] on monomeric PDI dianions (0.55), which indicates that at 100 μM **PDI-1**$^{2-}$ is partially assembled. We confirmed the latter by carrying out concentration dependent UV-Vis, which showed a progressive decrease of the I_{509nm}/I_{543nm} ratio upon dilution, thereby confirming that **PDI-1**$^{2-}$ is assembled at 100 μM. The latter experiments fit well to an isodesmic model with K_{eq} = 2.0 x 10^4 ± 3.0 x 10^3 M^{-1} (Fig. S4b, ESI†), though further studies are needed to confirm the exact mechanism of **PDI-1**$^{2-}$ assembly (section 5, ESI†). **PDI-1**$^{2-}$ assemblies of 96 ± 28 nm were also observed by dynamic light scattering (DLS) (Fig. 3c, **PDI-1**$^{2-}$).

Upon stirring in air, **PDI-1**$^{2-}$ was completely oxidized back to the neutral **PDI-1** in 2–3 min (Movie M1, ESI†). In agreement with previous reports, such reduction/oxidation cycle could be repeated at least 10 times (Movie M2, ESI†) without **PDI-1** decomposition (as assessed spectroscopically). Interestingly, the formation of the radical anion, **PDI-1**$^{\bullet-}$, resulted in a transient blue colour lasting for ~10 s (Movie M1, ESI†). In short, upon addition of $Na_2S_2O_4$ solution, colloidal assemblies of (as-prepared) **PDI-1** are reduced to **PDI-1**$^{\bullet-}$ and then to **PDI-1**$^{2-}$, leading to partial disassembly. This reduction step results in small **PDI-1**$^{2-}$ assemblies that are in equilibrium with **PDI-1**$^{2-}$ monomers. Upon oxidation in air, the latter process is reversed (i.e., **PDI-1**$^{2-}$ → **PDI-1**$^{\bullet-}$ → **PDI-1**) within minutes. The latter reduction / oxidation steps will be referred to as a redox cycle.

Next we studied the effect of a single redox cycle on the self-assembly of **PDI-1** (Fig. 1b, steps iii, iv, vi). Immediately after reduction to **PDI-1**$^{2-}$ (100 μM) no assemblies could be observed by confocal microscopy (not shown), since their size (i.e., 96 ± 28 nm) is below the detection limit. Upon air oxidation, red emitting assemblies of **PDI-1** reappeared, with a median size that evolved from ~400 nm to 1–2 μm in about 10 min, as evidenced by time-lapse microscopy (Fig. 2b,c). The final size of these assemblies (i.e., that went through 1 redox cycle) is smaller (and size distribution narrower) as compared to as-prepared **PDI-1** samples (Fig. 2a,b). UV-Vis spectra of the cycled assemblies show a less intense and blue-shifted absorption band with respect to as-prepared **PDI-1** solutions (compare Fig. 2d with Fig. S2a, ESI†), resembling reported PDIs stacks with 30° rotated chromophores.[18,19,26,27] The latter results indicate that **PDI-1** forms helical assemblies, as was recently shown by high-resolution TEM.[28]

During the assembly process (~10 min) the overall optical density (OD) increased, a clear red-shift of the peaks at 502 and 548 nm occurred (to 508 and 567 nm, respectively), and a new peak appeared at 528 nm (Fig. 2d). Since there is a considerable contribution of light scattering (see below) we show UV-Vis spectra in terms of optical density OD (i.e., accounting for scattering as well as absorption). The OD spectrum after 20 min (Fig. 2d, top red line) resembles again that of as-prepared **PDI-1** solutions (cf. Fig. 3d, **PDI-1**), indicating that the assembly process has finished.

AFM images (Fig. S5a, ESI†) of **PDI-1** solutions spin-coated on mica immediately after oxidation (i.e., from equilibrium i to oxidation ii in Fig. 1b) show fibrous aggregates with a regular height of 1.5 ± 0.1 nm (corresponding to twice the width *w* of **PDI-1**, Fig. 1a). On the other hand, samples of **PDI-1** spin-coated 20 min after oxidation (Fig. S5b, ESI†) show assemblies of fused smaller rigid rods, with a regular height of 2.1 ± 0.2 nm (i.e., 3 x *w*, Fig. 1a). Both the changes in the UV-Vis and AFM measurements point to a hierarchical growth process from initial 1D columnar assemblies of **PDI-1** (after ii, Fig. 1b) that assemble side-to-side to form fused bundles (iii and iv, Fig. 1b), in agreement with recent reports on structurally similar PDIs in water.[28] Moreover, the side-to-side fusing of 1D **PDI-1** stacks during the assembly process would affect the intracolumnar order, which could account for the changes observed in the UV-Vis spectra of Fig. 2d (i.e., a red shift and new peak at 528 nm). In fact, it is well known that the exciton coupling and the resulting spectral features are very sensitive to even minimal changes in the actual chromophore arrangement (e.g. distance or rotational offset).[18,26,28]

Interestingly, when following the time evolution of **PDI-1** assembly immediately after oxidation (i.e., steps iii, iv, v in Fig. 1b) the OD intensity at 528 nm was S-shaped (Fig. 2e). The latter observation suggests an autocatalytic (nucleated) process underlying the hierarchical growth of **PDI-1** assemblies (iii, Fig. 1b). To confirm this hypothesis, we followed the assembly kinetics (after 1 redox cycle) between 10 and 100 µM (cf. section 7, ESI†), and found that the assembly rates change drastically with concentration. We used a 2-step minimal autocatalytic model (step 1: A → B, and step 2: A + B → 2B, where B represents the species that contributes most to the OD) and obtained good fits to our S-shaped OD curves (cf. section 7, ESI†). However, this phenomenological model lumps all assembly events together into a nucleation phase (i.e., step 1) and elongation/growth phase (i.e., step 2), and is perhaps too simplistic. Stronger evidence comes from seeding experiments, where **PDI-1** assemblies of 1h old (obtained by performing 1 redox cycle) were added to a solution of just cycled **PDI-1**. In Fig. 2e it can be seen that at 10 µM there is long lag phase of ~10 min, and the total time to complete the assembly process is ~70 min. When 1h old seeds were added at the start the increase in OD is almost instantaneous and the plateau in OD is reached much faster (Fig. 2e). Moreover, if 1h old seeds were first sonicated (for 5 min) the growth is even faster, in agreement with nucleated growth.

So far, the molecular picture distilled from our results (steps i–v in Fig. 1b) is that i) upon reduction by $Na_2S_2O_4$, an equilibrium is established between monomeric and assembled **PDI-1**$^{2-}$, ii) oxidation of these **PDI-1**$^{2-}$ assemblies leads to small **PDI-1** structures with a different molecular packing, iii) nucleation occurs, which leads to iv) side-to-side fusion of 1D stacks, and v) results in precipitation (overnight).

Interestingly, we found that the **PDI-1** assemblies at 100 µM progressively change when doing more than one redox cycle, but only when cycled at a certain frequency (see section 2, ESI†). Specifically, when 7 cycles are performed at 3 min intervals—that is, without allowing time for hierarchical growth, which takes around 10 min at 100 µM—the resulting assemblies precipitate completely just as for as-prepared **PDI-1** samples (i.e., pathway i–v in Fig. 1b). However, when 7 (or more) cycles were performed at regular intervals of 20 min—that is, allowing time growth— only partial precipitation occurred, and a visibly pink supernatant was observed (Fig. S7, ESI†). The latter supernatant had a concentration of 10 µM (by UV-Vis) and was colloidally stable for months.

When studied in more detail, we observed that the scattered light intensity R_{vv}/c in DLS increased greatly when comparing the as-prepared **PDI-1** (dashed line in Fig. 3a) to samples that had undergone 1 redox cycle (red squares Fig. 3a). Upon further cycling we observed: i) a progressive decrease in R_{vv}/c (compare plateaus in Fig. 3a, labels 1 → 7), ii) an increase in the lag phase (Fig. 3b, red asterisks moving to the right), and iii) a continuous increase in OD (Fig. 3c). On the other hand, the size ($R_H \approx 628 \pm 83$ nm) and distribution of the assemblies

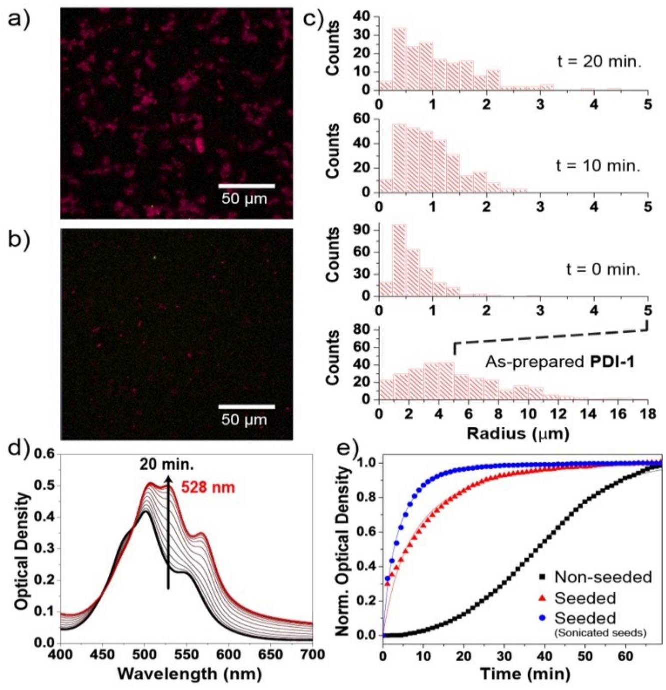

Fig. 2 Experiments after 1 redox cycle. (a,b) True colour confocal micrographs (using spectral detector) of 100 µM **PDI-1** solution: (a) as-prepared, (b) 20 min after 1 redox cycle. (c) Size distribution of **PDI-1** aggregates as-prepared (bottom) and at t = 0, 10, 20 min after 1 redox cycle (by particle analysis of micrographs). (d) UV-Vis spectra of a 100 µM **PDI-1** solution (optical path 2 mm) immediately after 1 redox cycle, showing a red shift and new peak at 528 nm. (e) Normalized optical density (OD) at 528 nm vs. time after 1 redox cycle for 10 µM **PDI-1** (black squares) and for 10 µM **PDI-1** seeded with 1h aged **PDI-1** seeds (red triangles), or sonicated seeds (blue circles). The S-shape indicates autocatalytic growth.

(20 min after each cycle) remained approximately constant typically after the third cycle.

The latter observations indicate changes in pathway selection upon cycling. Firstly, the decreasing scattering intensity R_{vv}/c and increasing OD point to progressive structural changes in the **PDI-1** assemblies after each cycle. Indeed, it confirms that the changes in OD observed in Fig. 2d are not only due to scattering (i.e., otherwise a decrease in R_{vv}/c should lead to a decrease in OD), but to a real chromophore rearrangement. Secondly, the increasing lag time shows that the nucleation (and thus likely the structure or number of nucleating species) is altered by multiple cycles. And lastly, a constant R_H and decreasing R_{vv}/c points to a denser packing of the **PDI-1** assemblies upon cycling. From these results we conclude that the frequency of redox cycling determines the balance between i) keeping the **PDI-1** molecules in solution (i.e., cycle faster than precipitation), and ii) providing enough time to allow for nucleation and growth of the assemblies. The key feature to achieve cycle-dependent pathway selection is that we do not allow the system to reach the **PDI-1**$^{2-}$ (pre)equilibrium (i, Fig. 1b) completely, which for longer times (in the reduced state) would "reset" the system and erase the memory of previous cycles.

Overall, our approach of using reducing ($Na_2S_2O_4$) and oxidizing agents (i.e., O_2) as chemical fuels to drive assembly and disassembly cycles can be used to better control pathway selection. Moreover, chemically fuelled self-assembly[29] can be used to overcome strong kinetic barriers thus allowing other strongly hydrophobic self-assembling moieties to be used in aqueous environments.

We thank the Region Alsace, University of Strasbourg Institute for Advanced Study (USIAS), ANR-10-LABX-0026_CSC, and Marie-Curie "NON-EQ-SA" for funding.

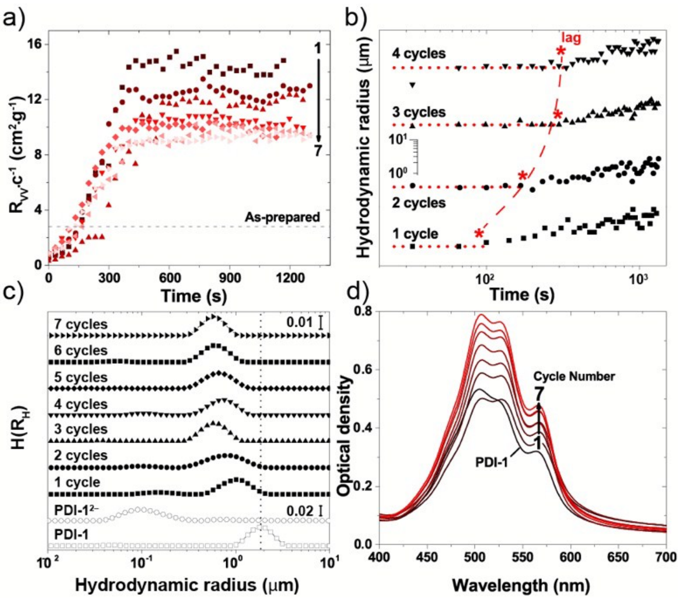

Fig. 3. Multiple redox cycle experiments. (a) Absolute scattering intensity R_{vv}/c vs time immediately after oxidation. The decreasing plateau indicates denser assemblies upon cycling (1→7). (b) Hydrodynamic radius R_H (from DLS) vs. time. Red stars (and dashed line) show increasing lag times upon cycling. (c) R_H measured for as-prepared 100 µM **PDI-1** (empty squares), **PDI-1**$^{2-}$ (empty circles) and for **PDI-1** (filled symbols) for up to 7 redox cycles show that after ~3 cycles the size of the assemblies remains constant. (d) UV-Vis spectra of **PDI-1** (each recorded 20 min after oxidation) increase upon cycling, showing internal structural changes in the **PDI-1** assemblies.

Notes and references

1 J.-M. Lehn, *Science*, 2002, **295**, 2400–2403.
2 T. Aida, E. W. Meijer and S. I. Stupp, *Science*, 2012, **335**, 813–817.
3 Y. Tidhar, H. Weissman, S. G. Wolf, A. Gulino and B. Rybtchinski, *Chem. – Eur. J.*, 2011, **17**, 6068–6075.
4 P. A. Korevaar, S. J. George, A. J. Markvoort, M. M. J. Smulders, P. A. J. Hilbers, A. P. H. J. Schenning, T. F. A. De Greef and E. W. Meijer, *Nature*, 2012, **481**, 492–496.
5 P. A. Korevaar, T. F. A. de Greef and E. W. Meijer, *Chem. Mater.*, 2014, **26**, 576–586.
6 F. Tantakitti, J. Boekhoven, X. Wang, R. V. Kazantsev, T. Yu, J. Li, E. Zhuang, R. Zandi, J. H. Ortony, C. J. Newcomb, L. C. Palmer, G. S. Shekhawat, M. O. de la Cruz, G. C. Schatz and S. I. Stupp, *Nat. Mater.*, 2016, **advance online publication**.
7 D. Chandler, *Nature*, 2005, **437**, 640–647.
8 L. Zang, Y. Che and J. S. Moore, *Acc. Chem. Res.*, 2008, **41**, 1596–1608.
9 T. M. Hermans, A. B. Maarten, N. Gomopoulos, A. F. Smeijers, B. Mezari, E. N. Van Leeuwen, M. R. Vos, P. C. Magusin, P. A. Hilbers, M. H. Van Genderen and others, *J. Am. Chem. Soc.*, 2007, **129**, 15631–15638.
10 T. M. Hermans, M. A. Broeren, N. Gomopoulos, P. Van Der Schoot, M. H. Van Genderen, N. A. Sommerdijk, G. Fytas and E. W. Meijer, *Nat. Nanotechnol.*, 2009, **4**, 721–726.
11 M. Numata, *Chem. - Asian J.*, 2015, **10**, 2574–2588.
12 A. Sorrenti, Z. El-Hachemi, J. Crusats and J. M. Ribo, *Chem. Commun.*, 2011, **47**, 8551–8553.
13 S. Ogi, K. Sugiyasu, S. Manna, S. Samitsu and M. Takeuchi, *Nat. Chem.*, 2014, **6**, 188–195.
14 S. Ogi, V. Stepanenko, K. Sugiyasu, M. Takeuchi and F. Würthner, *J. Am. Chem. Soc.*, 2015, **137**, 3300–3307.
15 Z. El-Hachemi, G. Mancini, J. M. Ribó and A. Sorrenti, *J. Am. Chem. Soc.*, 2008, **130**, 15176–15184.
16 D. Görl, X. Zhang, V. Stepanenko and F. Würthner, *Nat. Commun.*, 2015, **6**, 7009.
17 J. van Herrikhuyzen, A. Syamakumari, A. P. H. J. Schenning and E. W. Meijer, *J. Am. Chem. Soc.*, 2004, **126**, 10021–10027.
18 F. Würthner, C. R. Saha-Möller, B. Fimmel, S. Ogi, P. Leowanawat and D. Schmidt, *Chem. Rev.*, 2015.
19 D. Görl, X. Zhang and F. Würthner, *Angew. Chem. Int. Ed.*, 2012, **51**, 6328–6348.
20 S. Seifert, D. Schmidt and F. Würthner, *Chem Sci*, 2015, **6**, 1663–1667.
21 E. Shirman, A. Ustinov, N. Ben-Shitrit, H. Weissman, M. A. Iron, R. Cohen and B. Rybtchinski, *J. Phys. Chem. B*, 2008, **112**, 8855–8858.
22 R. O. Marcon and S. Brochsztain, *J. Phys. Chem. A*, 2009, **113**, 1747–1752.
23 M. A. Iron, R. Cohen and B. Rybtchinski, *J. Phys. Chem. A*, 2011, **115**, 2047–2056.
24 E. Krieg, E. Shirman, H. Weissman, E. Shimoni, S. G. Wolf, I. Pinkas and B. Rybtchinski, *J. Am. Chem. Soc.*, 2009, **131**, 14365–14373.
25 X. Cao, Y. Wu, H. Fu and J. Yao, *J. Phys. Chem. Lett.*, 2011, **2**, 2163–2167.
26 J. Seibt, P. Marquetand, V. Engel, Z. Chen, V. Dehm and F. Würthner, *Chem. Phys.*, 2006, **328**, 354–362.
27 Z. Chen, V. Stepanenko, V. Dehm, P. Prins, L. D. A. Siebbeles, J. Seibt, P. Marquetand, V. Engel and F. Würthner, *Chem. – Eur. J.*, 2007, **13**, 436–449.
28 X. Zhang, D. Görl, V. Stepanenko and F. Würthner, *Angew. Chem. Int. Ed.*, 2014, **53**, 1270–1274.
29 J. Boekhoven, W. E. Hendriksen, G. J. Koper, R. Eelkema and J. H. van Esch, *Science*, 2015, **349**, 1075–1079.